MOX–Report No. 61/2014

Elasto-capillarity controls the formation and the morphology of beads-on-string structures in solid fibres

Taffetani, M.; Ciarletta, P.

MOX, Dipartimento di Matematica "F. Brioschi"
Politecnico di Milano, Via Bonardi 9 - 20133 Milano (Italy)

mox@mate.polimi.it http://mox.polimi.it

Elasto-capillarity controls the formation and the morphology of beads-on-string structures in solid fibres

Matteo Taffetani[1] Pasquale Ciarletta[2]

December 16, 2014

[1] MOX, Dipartimento di Matematica, Politecnico di Milano Fondazione CEN
Piazza Leonardo da Vinci 32, I-20133 Milano, Italy
E-mail: `matteo.taffetani@polimi.it`

[2] MOX, Dipartimento di Matematica, Politecnico di Milano Fondazione CEN
Piazza Leonardo da Vinci 32, I-20133 Milano, Italy
CNRS and Institut Jean le Rond d'Alembert, UMR 7190, Université Paris 6
4 place Jussieu case 162, 75005 Paris, France
E-mail: `pasquale.ciarletta@upmc.fr`

Abstract

Beads-on-string patterns have been experimentally observed in solid cylinders for a wide range of material properties and structural lengths, from millimetric soft gels to nanometric hard fibres. In this work, we combine theoretical analysis and numerical tools to investigate the formation and the nonlinear dynamics of such beaded structures. We show that this morphological transition is driven by elasto-capillarity, i.e. a complex interplay between the effects of surface tension and bulk elasticity. Unlike buckling or wrinkling, the presence of an axial elongation is found here to favour the onset of fibre beading, in agreement with existing experimental results on electrospun fibres, hydrogels and nerves. Our results also prove that the applied stretch can be used in fabrication techniques to control the morphology of the emerging beads-on-string patterns. Such quantitative predictions open the way to several applications, from tissue engineering to the design of stretchable electronics and the micro-fabrication of functionalized surfaces.

Since the first experimental observation dating back to 1833 [1], it is well known that the surface tension in a liquid filament can trigger the transition into a varicose shape, followed by a sudden breakup into droplets. Linear stability studies [2, 3] have later proved that this phenomenon, thereafter named Rayleigh-Plateau instability (RPI), is governed by a competition between the surface tension, seeking to reduce the surface area at constant fluid volume, and the fluid inertia, opposing to motions over long distances. More recent developments have focused on understanding the nonlinear dynamics of the droplet formation in free-surface flows [4] and the formation of blistering patterns during the capillary thinning of viscoelastic solutions [5]. Although also elastic solids possess a surface tension, the influence of a capillary effect for their macroscopic shaping can be often neglected, since the formation of surface patterns is contrasted by the high bulk energy required for an elastic deformation. Nevertheless, capillary and elastic forces scale down very differently while decreasing the typical size L_s of the system [6], becoming comparable at low enough length-scales. In fact, if μ is the shear modulus of the material and γ is its surface tension, an elasto-capillary interaction can be observed if the characteristic length $L_{ec} = \gamma/\mu$ is of the same order of L_s. Since L_{ec} is in the sub-millimeter range [7], the ability of the surface tension to provoke a relevant deformation of a solid structure has been very recently observed in a number of miniaturized systems, such as the coalescence in wet hair clumps [8], the creation of complex microscopic structures through the wrapping of a liquid drop [9] or their pattern selection through a drop impact [10]. Moreover, an elasto-capillary effect at more macroscopic scales might also occur for very soft solids, thus decreasing μ and increasing L_{ec}, as recently observed by immerging centimeter-scale elastic rods, made of a gel just above the percolation threshold, into an aqueous solution [11].

Similarly to the RPI, it is therefore expected that elasto-capillary effects can drive the occurrence of a peristaltic pattern for elastic filaments with initial radius R_0 somewhat comparable to its capillary length L_{ec}. This morphological transition has been experimentally observed in applications spanning a wide range of elastic properties and characteristic lengths, from millimetric soft gel [12] to nanometric hard polymer fibres [13]. Although some theoretical analysis and empirical correlations have been recently proposed [14, 15], the effects of elasto-capillarity on the resulting beaded morphology in solids are barely understood. In particular, whilst it is well known that a compressive strain triggers many classical elastic instabilities, such as wrinkling [16] or buckling [17, 18], it is yet unclear why the axial elongation of a capillary elastic filament favors the onset of beading. This has been observed in few experiments with soft cylinders having very different physical and structural characteristics, including electrospun fibers [19], hydrogels [20] and nerve axons [21, 22], as depicted in Fig. 1. In this perspective, this work aims at investigating how bulk elasticity and surface tension concur for driving a beading instability in soft elastic fibres, evaluating the onset conditions and its dynamics far from the bifurcation point. In particular, the main goal is to prove insights on the effects of the elasto-capillarity on the onset and the nonlinear dynamics of the beaded patterns, opening new possibilities for generating controllable beads-on-string structures in a wide range of experimental applications. With this scope, both a theoretical analysis and numerical tools are proposed in the following to provide a quantitative prediction of the beaded morphology in the fully nonlinear regime.

Let us consider an elastic cylinder with radius R_0 and axial length L_0 subjected to an axial strain λ_z, so that (r, z) and (R, Z) are the polar coordinates in the spatial and material settings, respectively. Assuming that the filament is made of a neo-Hookean incompressible material with density ρ, three energy contributions can be taken into account: (i) the kinetic energy $K = (1/2)\int_{Z=0}^{L_0} dZ \int_{R=0}^{R_0} dR \rho \mathbf{v}^2$ where $\mathbf{v}$ is the spatial velocity; (ii) the bulk elastic energy $U_{el} = (\mu/2)\int_{Z=0}^{L_0} dZ \int_{R=0}^{R_0} dR\,(J_1 - 3)$, where $J_1 = \left[2 + \sum_j u_{i,j}^2 + 2u_{i,i} + (1 + u_r/r)^2\right]$, u_i indicates the component of the displacement along the direction i, with (i, j) spanning over (r, z), comma denotes partial derivative and the Einstein summation rule on dummy indices is considered; (iii) the capillary energy on the free surface $U_{surf} = \gamma \int_{z=0}^{\lambda_z L_0} dz r \sqrt{1 + r_{,z}^2}$. Using a variational approach, the equilibrium of the elastic filament arises from the minimization of the total energy by imposing a null variation of the Lagrangian functional L as

$$\delta L = \delta(K - U_{el} - U_{surf}) = 0 \tag{1}$$

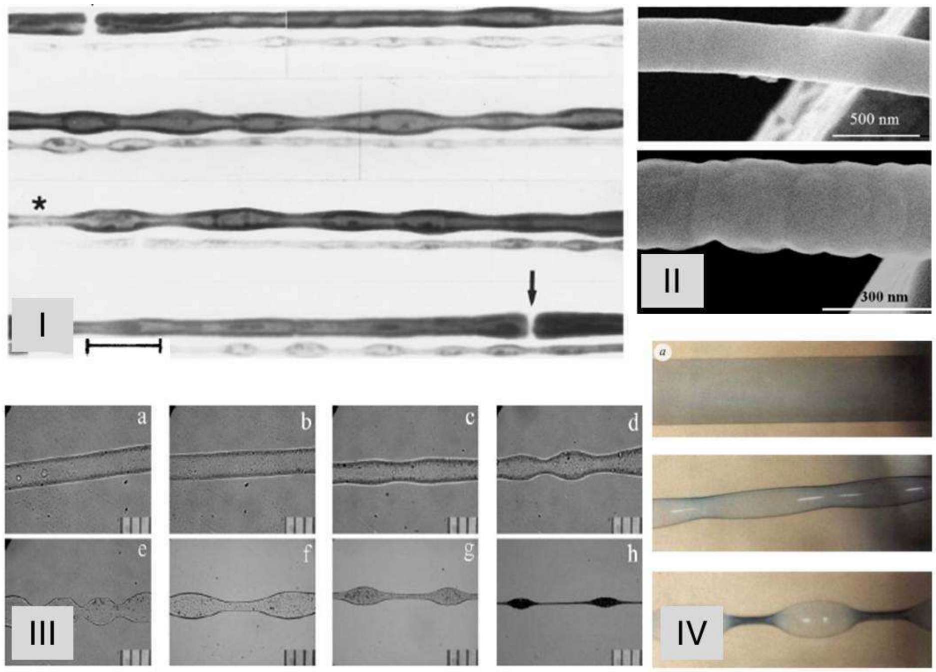

Figure 1: Bead-on-string patterns in solid fibers with different underlying physical properties: (I) The rat sciatic nerve can be considered as a cylinder with radius of few μm: applying an axial stretch, the nerve first loses the typical banding observed at its rest condition (bands of Fontana), later developing a beading instability after a threshold value of the elongation ratio. A further increase of the stretch provokes an initial increase of the beads amplitudes, which later saturate to a constant value, after which beading gradually disappears. The scale bar is 50 μm (from [23]). (II) Nanofibres are cylindrical structures having radii of the order of hundreds of nm and characterized by a small aspect ratio R_0/L; if elongated, an initially circular filaments can undergo a beading instability (from [13]). (III) Electrospinning is a technique used for the production of polymeric fibres based on an extrusion process. The morphology of the extruded fibres is affected by several experimental parameters. In particular, it is shown that increasing the collecting distance from (a) to (h), i.e. increasing the applied stretch, promotes the onset of beading. Each division in the scale bar corresponds to 10 μm (from [25]). (IV) Soft cylindrical gels with radii of few mm have a very complex morphological diagram. In particular, Matsuo and Tanaka [20] reported that the application of a finite axial stretch can promote the occurrence of a bubble/beaded pattern (from [20]).

The incompressibility constraint can be exactly fulfilled using a stream function $\phi = \phi(R, z, t)$ in a mixed coordinate state [14], so that $r^2 = 2\phi_{,z}$ and $Z = (1/R)\phi_{,R}$. Accordingly, the basic axis-symmetric solution after imposing the axial stretching λ_z is given by $\phi_0(R, z, t) = (1/(2\lambda_z))\, R^2\, z$. In order to perform a stability analysis of this static solution, let us consider a perturbation of the stream function as:

$$\phi(R, z, t) = \phi_0 + \sum_{n=1}^{\infty} \epsilon^n R \phi_n\, (R, z, t) \tag{2}$$

where ϵ is a small order parameter to be defined. Assuming variable separation, we look for a linear order solution in the form of a travelling wave with axial velocity V, being $\phi_1(R,z,t) = u^{(1)}\left(R/\sqrt{\lambda_z}\right)e^{Ik(z-Vt)} + c.c.$, where I is the imaginary unit, $c.c.$ indicates the complex conjugate, and $k = (2\pi m)/L_0$ is the axial wavenumber of the perturbation, having integer mode m. Using Eq. (2), the bulk equilibrium from Eq. (1) reads

$$\mathcal{L}_1\left[\mathcal{L}_q\left(u\left(r\right)\right)\right] = 0 \tag{3}$$

where $\mathcal{L}_p = \partial_r^2 + (1/r)\partial_r - (1/r^2) - (k^2p^2)$ for $p = (1,q)$, and $q = \sqrt{\lambda_z\left(\lambda_z^2 - \frac{V^2}{c^2}\right)}$ with $c = \sqrt{\mu/\rho}$ being the speed of sound in the material.

Imposing regularity for $r = 0$ and considering the boundary conditions $r_0 = R_0/\sqrt{(\lambda_z)}$, the solution of Eq. (3) can be written as

$$u^{(1)}\left(r\right) = \frac{I_1\left(krq\right)}{I_1\left(kr_0q\right)} - \left(\frac{\lambda_z^3+1}{2}\right)\frac{I_1\left(kr\right)}{I_1\left(kr_0\right)} \tag{4}$$

where I_n is the modified Bessel function of order n. Moreover, the dispersion relation for a static critical wave with $V = 0$ reads

$$2\frac{(\lambda_z^3-1)}{\lambda_z^{\frac{3}{2}}} + \bar{k}\left[\frac{4}{\lambda_z^{\frac{1}{2}}}\frac{I_0\left(\bar{k}\lambda_z\right)}{I_1\left(\bar{k}\lambda_z\right)} - \frac{\left(\lambda_z^3+1\right)^2}{\lambda_z^2}\frac{I_0\left(\frac{\bar{k}}{\sqrt{\lambda_z}}\right)}{I_1\left(\frac{\bar{k}}{\sqrt{\lambda_z}}\right)}\right] + \frac{L_{ec}}{R_o}\left(\lambda_z^3-1\right)\left(1-\frac{\bar{k}^2}{\lambda_z}\right) = 0 \tag{5}$$

where $\bar{k} = kR_0$ is the dimensionless wavenumber. The marginal stability curves from Eq. (5) are depicted as solid lines in Fig. 2, showing the critical axial stretch λ_z^{th} as a function of the elasto-capillary ratio L_{ec}/R_0 for varying $\bar{k}$. In particular, it is found that the marginal stability curves superimpose for $\bar{k} < 0.01$, thus predicting the onset of a long wavelength beading. In absence of an axial strain, i.e. $\lambda_z = 1$, the instability threshold is given by $L_{ec} = 6R_0$ [24]. Instead, if the cylinder is elongated, i.e. $\lambda_z > 1$, the beading instability can occur at lower elasto-capillary ratios L_{ec}/R_0 up to a minimum value given by $(L_{ec}/R_0)_{min} = 5.66$. This novel theoretical result confirms the elasto-capillary effect reported in the experimental observations of Fig. 1, giving analytical predictions on the required axial stretching for driving the onset of beading in an elastic filament with $L_{ec}/R_0 > (L_{ec}/R_0)_{min}$. Experimental data on the fabrication of nanofibres by electrospinning have evidenced this elasto-capillary effect [19, 25]; considering the typical surface tension in the range $\gamma = 20 - 70mN/m$ and a characteristic radius of $R_0 = 125nm$, it has been shown that the formation of beads can be triggered by increasing the surface tension (i.e. L_{ec}) above a critical value of about $\gamma = 59.3mN/m$ [19], which from our theoretical prediction of L_{ec} in the range $[5.66 - 6]R_0$ correspond to a shear modulus of about $\mu = 80 - 85kPa$, in agreement with the experimental measures [15]. The favouring effect of axial stretching on the formation of beading is also experimentally confirmed varying the applied electric field at fixed collecting distance reporting beading for lower elasto-capillary ratios, i.e. $(L_{ec}/R_0)_{min} < L_{ec}/R_0 < 6$, together with a morphological change from spindle- to sphere-like beads [26, 27]. In order to study the dynamics of pattern formation of the beading instability, let us first perform a weakly non-linear analysis using the multiple-scale method. Assuming a small increase of the axial stretch above the instability threshold, such that $\epsilon = \sqrt{(\lambda_z - \lambda_z^{th})/\lambda_z^{th}} << 1$, the linear stability analysis predicts that the velocity of the near-critical wave is given by $V = \sqrt{3}(c\lambda_z^{th})\epsilon$. If we define a characteristic time $t_c = R_0/V$, the linear perturbation can be rewritten as $\phi_1(R,z,t) = A(\tau)u^{(1)}\left(R/\sqrt{\lambda_z}\right)e^{Ikz} + c.c.$, where $\tau = \epsilon\,(t/t_c)$ is the slow time-scale describing the growth of the amplitude $A(\tau)$ of the near-critical beads, that cannot be fixed by a linear analysis. In order to study the evolution of the beading beyond the instability threshold, we can extend the series development in Eq. (2) up to the third order in ϵ (n=3), taking into account the expression of the lower order terms to generate the resonating terms at higher orders. A solvability condition for the amplitude $A(\tau)$ can be obtained by considering that the total mechanical energy E of the system must be conserved in absence of dissipative processes [28], so that

$$\frac{dE}{dt} = \frac{d}{dt}\left[K + U_{el} + U_{surf}\right] = 0 \tag{6}$$

Imposing Eq. (6) at the forth order in ϵ allows deriving the evolution law (also known as Ginzburg-Landau equation) driving the growth of the beading amplitude in the weakly nonlinear regime, being

$$\kappa\partial_\tau^2 A(\tau) + \nu A(\tau) - \psi\left|A(\tau)\right|^2 A(\tau) = 0 \tag{7}$$

where κ and ν only depend on the linear order solution, ψ is a complex function of the higher order terms, and the conjugate equation also applies. The amplitude Eq. (7) proves that the beading occurs after a pitchfork bifurcation: if $\nu/\psi > 0$, there exists a stable solution $A^{st} = \sqrt{\nu/\psi}$, so that the amplitude regularly grows as the square root of the distance from the critical stretch threshold, i.e. as ϵB^{st} with $B^{st} = 2k\sqrt{\lambda_z}u(R_0)A^{st}$(supercritical bifurcation); if $\nu/\psi < 0$, the pitchfork is unstable and one expects that the solution has a discontinuity, jumping into a stable configuration which is driven by nonlinear effects of higher orders (subcritical bifurcation). In particular, it is found that the bifurcation turns supercritical when increasing both the critical wavenumber $\bar{k}^{th} = 2\pi R_0/L_0$ and the critical axial stretch λ_z^{th} at the onset of the instability. This means that the beading becomes continuous and controllable when applying a finite axial stretch to a solid cylinder with an aspect ratio R_0/L_0 beyond a given (small) value. Conversely, the instability can be weakly nonlinear unstable for very slender filaments: thus the analytical results predict a discontinuous beading formation just above the linear stability threshold, later controlled by nonlinearities. Indeed, the nature of bifurcation can be theoretically evaluated by studying the coefficients ν and ψ in Eq. (7). These parameters depend on the functions $\phi_n(R,z,t)$ describing the perturbation of the stream function in Eq. (2). In particular, their whole expressions are the following:

$$\begin{gathered}\phi_1(R,z,t) = \\ Ru^{(1)}\left(R/\sqrt{\lambda_z}\right)\left[A(\tau)e^{Ikz} + A^*(\tau)e^{-Ikz}\right]\end{gathered} \tag{8}$$

$$\begin{gathered}\phi_2(R,z,t) = Ru^{(2)}\left(R/\sqrt{\lambda_z}\right)\left[A(\tau)A^*(\tau)\right] \\ +Rw^{(2)}\left(R/\sqrt{\lambda_z}\right)\left[A^2(\tau)Ie^{2Ikz} - A^{*2}(\tau)Ie^{-2Ikz}\right]\end{gathered} \tag{9}$$

$$\begin{gathered}\phi_3(R,z,t) = \\ Ru^{(3)}\left(R/\sqrt{\lambda_z}\right)\left[A^2(\tau)A^*(\tau)e^{Ikz} + A(\tau)A^{*2}(\tau)e^{-Ikz}\right] \\ +Rw^{(3)}\left(R/\sqrt{\lambda_z}\right)\left[A^3(\tau)e^{3Ikz} + A^{*3}(\tau)e^{-3Ikz}\right]\end{gathered} \tag{10}$$

where the superscript * indicates the complex conjugate. The functions $u^{(n)}$ and $w^{(n)}$, with $n = 1, 2, 3$, are obtained by solving the Euler Lagrange problem at order n in Eq. (1). Their analytical expressions is very cumbersome and is not reported in here for sake of simplicity. Numerical integrations allow to calculate the parameters ν and ψ, as reported in Table 1. The numerical values of the weakly non-linear coefficients correspond to linear stability thresholds depicted as squared markers in Fig. 2(a). It can be shown that the nature of the bifurcation changes varying the geometry of the fibre and its constitutive properties: controllable patterns can be obtained increasing the aspect ratios (R_0/L_0) and if the elasto-capillary length L_{ec} is farther from the stability limit without stretch.

Table 1: Numerical values of weakly non-linear coefficients ν and ψ in Eq. (7) and nature of the bifurcation (sub: subcritical; super: supercritical) obtained for cases in which $\mu = 20kPa$ and $R_0 = 0.2\mu m$. The results correspond to linear stability thresholds depicted as squared markers in Fig. 2(a).

$\frac{L_{ec}}{R_0}$	ν			ψ			$nature\ of\ bifurcation$		
	$\bar{k} = 0.01$	$\bar{k} = 0.1$	$\bar{k} = 0.2$	$\bar{k} = 0.01$	$\bar{k} = 0.1$	$\bar{k} = 0.2$	$\bar{k} = 0.01$	$\bar{k} = 0.1$	$\bar{k} = 0.2$
6.2	-	-	-0.232	-	-	0.042	-	-	sub
6.1	-	-	-3.303	-	-	0.798	-	-	sub
6.0	-	-0.231	-9.493	-	0.025	-16.32	-	sub	super
5.9	-0.059	-1.704	-18.47	0.019	1.307	-811.8	sub	sub	super
5.8	-0.275	-5.106		0.461	6.669		sub	sub	
5.75	-0.464	-7.361		1.369	-18.16		sub	super	
5.7	-0.686			3.156			sub		

We have investigated the fully non-linear dynamics of stretch-induced beading in solid cylinders implementing the elasto-capillary problem on a finite element code. Numerical simulations are carried out by using the open source software FEniCS for solving partial differential equations [29]. To guarantee the incompressibility constraint, a mixed formulation with triangular Taylor-Hood elements is implemented and the solution has been found through an incremental iterative Newton-Raphson methods with direct solver. The results of the numerical simulations are first validated versus the theoretical results of the linear stability analysis, as depicted in Fig. 2, where the numerical thresholds are indicated by the square markers.

A morphological phase diagram from the simulations on the stretched cylinder is reported in Fig. 2(b), showing the nonlinear evolution of beading in different paths mimicking two different experimental settings. The path (A-B-C-D) in Fig. 2(b) concerns the application of an axial elongation at constant elasto-capillary ratio, and corresponds to the stretching experiments shown in Fig. 1(I,II). The numerical results indicate a smooth growth of beads beyond the critical stretch λ_z^{th}, whose amplitudes later saturate to a constant value whilst their spacing increases with an increasing axial strain. This morphological transition corresponds to the experimental observations on nerve axons (see Fig. 1(I)), where the application of an axial stretch of about 10% triggers the formation of beaded structures evolving at almost fixed amplitude over a certain range of applied stress before disappearing. However, it must be reminded that the use of a capillary energy is here a simplification of the elastic response of the outer membrane. Indeed, although a skin effect arises since the membrane thickness is much

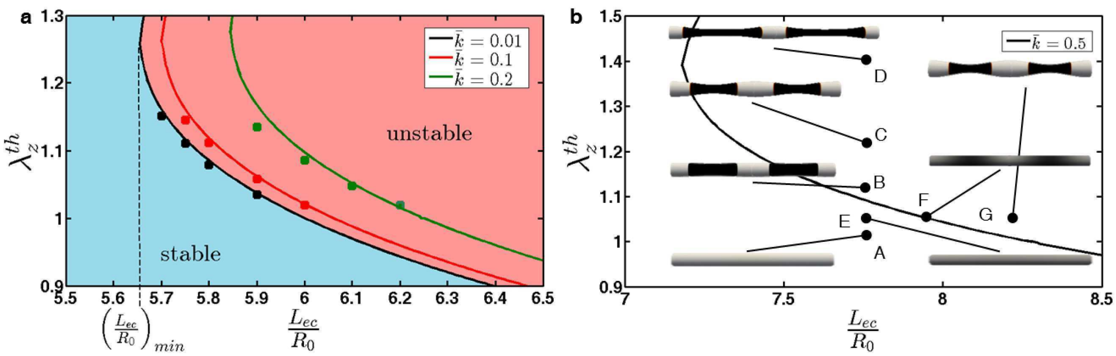

Figure 2: (a) Dispersion curves (solid lines) showing the critical axial stretch λ_z^{th} versus the elasto-capillary ratio L_{ec}/R_0 at varying $\bar{k}$. The squares indicate the thresholds computed numerically. (b) Morphological phase diagrams from the numerical simulations of two different paths, fixing $L_{ec}/R_0 = 7.7$ (A-B-C-D) and $\lambda_z = 1.05$ (A-E-F-G).

smaller than the radius of the nerve axon [21], a more accurate modelling of the membrane structure should include an elastic contribution in the corresponding surface energy.
The same behaviour is observed by stretching polyacrylonitrile (PAN) nanofibres (see Fig. 1(II)), where ripples develop after a critical stretch of $\lambda_z^{th} = 1.15$, which in our theoretical prediction gives an elasto-capillary ratio of about $L_{ec}/R_0 = 5.75$. Since PAN fibres are characterized by a surface tension $\gamma = 0.025 - 0.1N/m$ and $R_0 = 300 - 600nm$, such a prediction corresponds to a shear modulus in the range $\mu = 6 - 60kPa$, which is consistent with the reported data [30]. Such experimental values of λ_z^{th} and L_{ec}/R_0 have been used in numerical simulations in order to perform a quantitative comparison of the pattern dynamics. The resulting curves are depicted in Fig. 3, showing both the beading amplitude and their relative width versus the imposed stretch. In particular, ripples with amplitude of the order of magnitude of tents of nanometers are obtained, which correspond to the experimental observations [13]. Moreover, it is also confirmed that the beads amplitude initially grows as the square root of the distance from the critical thresholds, as predicted by our weakly nonlinear analysis (solid lines in Fig. 3(b)). Interestingly, whilst the amplitude is almost constant, the beading width decreases linearly with increasing axial stretch, as shown in Fig. 3(c). This is a very important finding, proving that the applied stretch can be used to control the resulting morphology of elasto-capillary fibres in tensile experiments. Conversely, the path (A-E-F-G) in Fig. 2(b) aims at mimicking the experiments of Matsuo and Tanaka [20], where dried cylindrical gels, with an initial radius R_0 in the range $0.35 - 0.5$ mm, are first stretched and then put in a water-acetone mixture, thus increasing the surface tension above the critical value for the elasto-capillary ratio L_{ec}/R_0. A bubble pattern is there observed for critical axial elongations λ_z^{th} up to 20%, which in our theoretical analysis correspond to a gel shear modulus of tens of Pa for a surface tension of $\gamma = 25mN/m$ [31], consistent with recent experimental measures [11]. However, it is important to underline that is would be more accurate to use a diffuse interface energy (e.g. of the Ornstein-Zernicke type) to model such experiments, although a capillary energy is an acceptable modelling simplification when the correlation length is much smaller than the radius. The numerical results on the pattern dynamics are also qualitatively consistent with these experiments, reporting a bead change

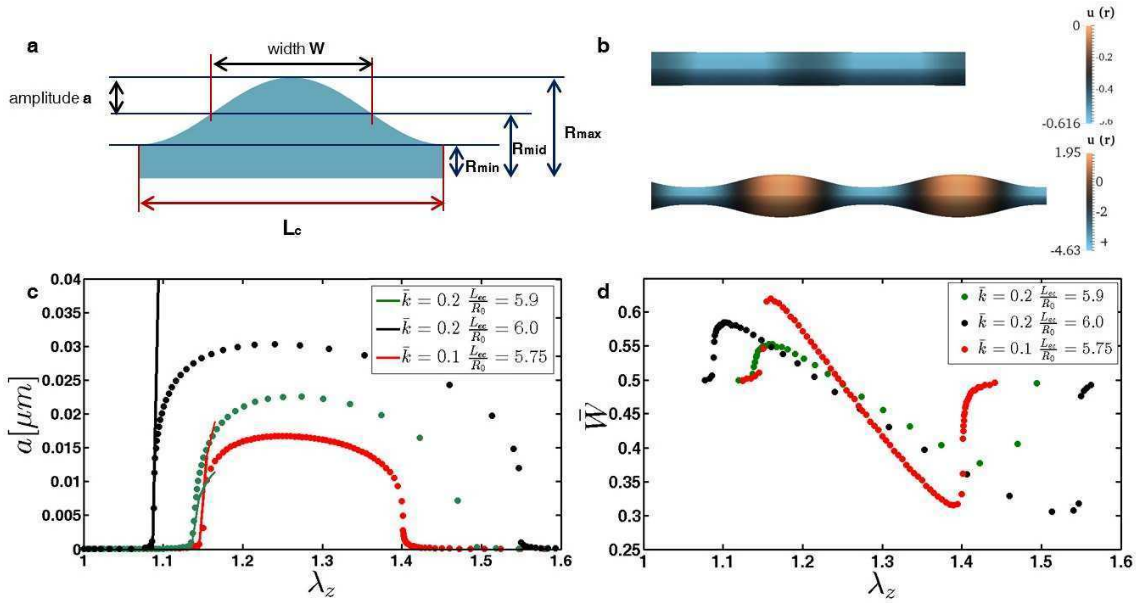

Figure 3: (a) Beading amplitude a and axial width W . (b) Numerical simulation mimicking the experiments on PAN nanofibres with $R_0 = 300nm$ [13] giving (c) the amplitude a and (d) the dimensionless width $\bar{W} = W/L_c$ for three different elasto-capillary ratios. Numerical data (circles) in (c) fit very well the theoretical predictions (solid lines) given by ϵB^{st} (solid lines) with no adjustable parameters: green line, $SSE = 1.59 \cdot 10^{-5}$; black line, $SSE = 3.47 \cdot 10^{-3}$; red line, $SSE = 3.10 \cdot 10^{-4}$ (SSE: summed square of residuals).

from spindle-like to sphere-like whilst increasing the surface tension at fixed applied stretch. A continuous variation of the bead amplitude was also recently reported [12] in absence of an axial strain, thus suggesting the occurrence of a supercritical bifurcation.
Nevertheless, the results of our weakly nonlinear analysis suggest that the beading instability is strongly dependent on the elasto-capillary properties and on the geometry of the solid cylinder. In particular, the fully nonlinear simulations confirmed that the bifurcation can turn subcritical in very slender cylinders, as shown in Fig. 3. In this case, the beading amplitude for short-wavelength perturbations is found undergoing a sharp variation after the linear stability threshold, suddenly jumping into a finite value. Moreover, a hysteresis loop is observed if the applied stretch is gradually removed (path A-B-C-D in Fig. 4, although the instability is totally reversible. Both these features are indicative signs of a subcriticality of the elasto-capillary instability, which is rather uncommon in elasticity [32].

Albeit our theoretical predictions indicate that the wavelength of beading scales in general as the length L_0 of the solid cylinder, they also predict that shorter undulations have very close instability thresholds for very slender filaments. Accordingly, the wavelength selection might be driven by the presence of surface defects in the real practice, as found for wrinkling [33]. Thus, an imperfection-sensitivity analysis of beading should be performed in a future study. Further developments will also focus on the effect of other interaction potentials (e.g. electrostatic, magnetic or intermolecular forces) on beading at lower scales of investigation.

In summary, we have presented both a theoretical and a numerical investigation of the

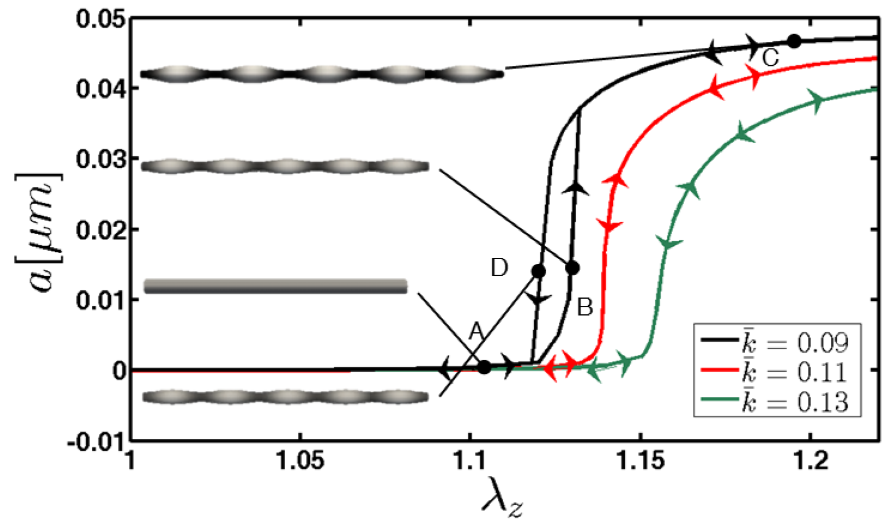

Figure 4: The beading amplitude a versus the applied axial stretch in a loading-unloading cycle for different wavenumbers $\bar{k}$, setting $R_0 = 0.24\mu m$, $L_0 = 80\mu m$, $\mu = 20kPa$, $\gamma = 0.028N/m$ ($L_{ec}/R_0 = 5.7$).

elasto-capillary effects driving beading instability in solid cylinders. Although our model does not claim describing all the underlying physical characteristics of the mentioned experiments, it proves that either the axial stretch λ_z or the elasto-capillary ratio L_{ec} control the beaded morphology over a large range of material properties and characteristic length-scales. Proposing for the first time a weakly nonlinear analysis for a nonlinear elastic cylinder, quantitative predictions are given on the effects of the geometrical and the elasto-capillary characteristics on the beading dynamics far from the bifurcation point. Thus, the results of this work can be used as guidelines for the fabrication of controllable patterns in a number of applications. Possible outcomes in material science concern the production of functional micro-threads in biomaterials, e.g. for mimicking the beads-on-string spider web [34], as well as the design of nanowires with tunable properties for stretchable electronics [35] or for sensor devices in micro-electro-mechanical systems [36]. Finally, the possibility to control the beading morphology opens new perspectives in many biological applications, from regenerative tissue engineering [37] to the fabrication of functionalized surfaces for cell culturing [38].

References

[1] F. Savart. Mmoire sur la constitution des veines liquides lances par des orifices. *Ann. Chim. Phys.*, 53: 337-374, (plates in Vol. 54), 1883.

[2] J. Plateau. Experimental and Theoretical Statics of Liquids Subject to Molecular Forces Only, Gauthier-Villars, 1873.

[3] Lord Rayleigh. On the instability of jets. *Proc. London Math. Soc.*, 1:4-13, 1878.

[4] J. Eggers. Nonlinear dynamics and breakup of free-surface flows. *Rev. Mod. Phys.*, 69: 865, 1997.

[5] R. Sattler, C. Wagner and J. Eggers. Blistering pattern and formation of nanofibers in capillary thinning of polymer solutions. *Phys. Rev. Lett.*, 100:164502, 2008.

[6] J.W. Van Honschoten, N. Brunets and N.R. Tas. Capillarity at the nanoscale. *Chem. Soc. Rev.*, 39:1096-1114, 2010.

[7] B. Roman and J. Bico. Elasto-capillarity: deforming an elastic structure with a liquid droplet. *J. Phys. Condens. Matter*, 22:493101, 2010.

[8] J. Bico, B. Roman, L. Moulin and A. Boudaoud. Elastocapillary coalescence ion wet hair. *Nature*, 432:690, 2004.

[9] C. Py, P. Reverdy, L. Doppler, J. Bico, B. Roman and C.N. Baroud. Capillary origami: spontaneous wrapping of a droplet with an elastic sheet. *Phys. Rev. Lett.*, 98:156103, 2007.

[10] A. Antkowiak, B. Audoly, C. Josserand, S. Neukirch and M. Rivetti. Instant fabrication and selection of folded structures using drop impact. *PNAS* 108:10400, 2011.

[11] S. Mora, C. Maurini, T. Phou, J.M. Fromental and Y. Pomeau. Solid drops: Large capillary deformations of immersed elastic rods. *Phys. Rev. Lett.* 111:114301, 2013.

[12] S. Mora, T. Phou, J.M. Fromental, L.M. Pismen and Y. Pomeau. Capillarity driven instability of a soft solid. *Phys. Rev. Lett.*, 105:214301, 2010.

[13] M. Naraghi, I. Chasiotis, H. Kahn, Y. Wen and Y. Dzenis. Mechanical deformation and failure of electrospun polyacrylonitrile nanofibers as a function of strain rate. *Appl. Phys. Lett.*, 91:151901, 2007.

[14] P. Ciarletta and M. Ben Amar. Peristaltic patterns for swelling and shrinking of soft cylindrical gels. *Soft Matter* 8:1760-1763, 2012.

[15] J.H. Yu, S.V. Fridrikh and G.C. Rutledge. The Role of Elasticity in the Formation of Electrospun Fibers. *Polymer*, 47:4789-4797, 2006.

[16] F. Brau, H. Vandeparre, A. Sabbah, C. Poulard, A. Boudadoud and P. Damman. Multiple-length-scale elastic instability mimics parametric resonance of nonlinear oscillators. *Nature Phys.*, 7:56-60, 2011.

[17] K. Krieger. Extreme mechanics: Buckling down. *Nature*, 488:146-147, 2012.

[18] P. Ciarletta. Buckling Instability in Growing Tumor Spheroids. *Phys. Rev. Lett.*, 110:158102, 2013.

[19] H. Fong, I. Chun and D.H. Reneker. Beaded nanofibers formed during electrospinning. *Polymer*, 40:4585-4592, 1999.

[20] F.S. Matsuo and T. Tanaka. Patterns in shrinking gels. *Nature*, 358:482-485, 1992.

[21] S. Ochs, R. Pourmand, R.A. Jersild and R.N. Friedman. The origin and nature of beading. *Prog. Neurobiol.*, 52:391-426, 1997.

[22] R. Pourmand, S. Ochs and R.A. Jersild Jr. The relation of the beading of myelinated nerve fibers to the bands of Fontana. *Neuroscience*, 61:373-380, 1994.

[23] V.S. Markin, D.L. Tanelian, R.A. Jersild Jr and S. Ochs. Biomechanics of stretch-induced beading. *Biophys. J.*, 76:2852-2860, 1999.

[24] B. Barriere, K. Sekimoto and L. Leibler. Peristaltic instability of cylindrical gels. *J. Chem. Phys.*, 105:1735-1738, 1996.

[25] W. Zuo, M. Zhu, W. Yang, H. Yu, Y. Chen and Y. Zhang. Experimental study on relationship between jet instability and formation of beaded fibers during electrospinning. *Polym. Eng. Sci.*, 45:704-709, 2005.

[26] J. M. Deitzel, J. Kleinmeyer, D. Harris and N.C. Beck Tan. Controlled deposition of electrospun poly (ethylene oxide) fibers. *Polymer*, 42:261-272, 2001.

[27] S. Ramakrishna, K. Fujihara, W.E Teo, T.C. Lim, Z. Ma. An Introduction to Electrospinning and Nanofibers, World Scientific Publishing Company, 2005.

[28] Y.B. Fu and R.W. Ogden. Nonlinear stability analysis of pre-stressed elastic bodies. *Continuum Mech. Therm.*, 11:141-172, 1999.

[29] A. Logg, K.A. Mardal and G.N. Wells. Automated Solution of Differential Equations by the Finite Element Method, Springer, 2012.

[30] X.F. Wu, Y.Y. Kostogorova-Beller, A.V. Goponenko, H. Hou and Y.A. Dzenis Rippling of polymer nanofibers. *Phys. Rev. E*, 78:061804, 2008.

[31] W. Shuhui and R.A. Shanks. Solubility study of polyacrylamide in polar solvents. *J. Appl. Polym. Sci.*, 93:1493-1499, 2004.

[32] J. S. Biggins, B. Saintyves, Z. Wei, E. Bouchaud and L. Mahadevan. Digital instability of a confined elastic meniscus. *PNAS*, 110:12545, 2013.

[33] Y. Cao and J.W. Hutchinson. From wrinkles to creases in elastomers. *Proc. R. Soc. A*, 468:94-115, 2012.

[34] V. Sahni, D.V. Labhasetwar and A. Dhinojwala. Spider Silk Inspired Functional Microthreads. *Langmuir*, 28:2206-2210, 2012.

[35] Y. Sun, W.M. Cho, H. Jiang, Y.Y. Huang and J.A. Rogers. Controlled buckling of semiconductor nanoribbons for stretchable electronics. *Nat. Nanotechnol.*, 1:201-207, 2006.

[36] J.A. Rogers and Y. Huang. A curvy, stretchy future for electronics. *PNAS*, 106:10875, 2009.

[37] P. Wallin, C. Zanden, B. Carlberg, N.H. Erkenstam, J. Liu and J. Gold. A method to integrate patterned electrospun fibers with microfluidic systems to generate complex microenvironments for cell culture applications. *Biomicrofluidics*, 6:024131, 2012.

[38] V. Beachley and X. Wen. Polymer nanofibrous structures: Fabrication, biofunctionalization, and cell interactions. *Prog. Polym. Sci.*, 35:868-892, 2010.

MOX Technical Reports, last issues

Dipartimento di Matematica "F. Brioschi",
Politecnico di Milano, Via Bonardi 9 - 20133 Milano (Italy)

61/2014 Taffetani, M.; Ciarletta, P.
Elasto-capillarity controls the formation and the morphology of beads-on-string structures in solid fibres

59/2014 Manzoni, A.; Pagani, S.; Lassila, T.
Accurate solution of Bayesian inverse uncertainty quantification problems using model and error reduction methods

60/2014 Signorini, M.; Micheletti, S.; Perotto, S.
CMFWI: Coupled Multiscenario Full Waveform Inversion for seismic inversion

58/2014 Menafoglio, A.; Secchi, P.; Guadagnini, A.
A Class-Kriging predictor for Functional Compositions with Application to Particle-Size Curves in Heterogeneous Aquifers

57/2014 Giverso, C.; Verani, M.; Ciarletta P.;
Branching instability in expanding bacterial colonies

56/2014 Antonietti, P. F.; Sarti, M.; Verani, M.; Zikatanov, L. T.
A uniform additive Schwarz preconditioner for the hp-version of Discontinuous Galerkin approximations of elliptic problems

55/2014 Antonietti, P. F.; Houston P.; Sarti, M.; Verani, M.
Multigrid algorithms for hp-version Interior Penalty Discontinuous Galerkin methods on polygonal and polyhedral meshes

54/2014 Ferrario, E.; Pini, A.
Uncertainties in renewable energy generation systems: functional data analysis, monte carlo simulation, and fuzzy interval analysis

53/2014 Ieva, F.; Paganoni, A.M., Pietrabissa, T.
Dynamic clustering of hazard functions: an application to disease progression in chronic heart failure

52/2014 Dede , L..; Quarteroni, A.; S. Zhu, S.
Isogeometric analysis and proper orthogonal decomposition for parabolic problems